Fabrication and Operation of SMPM Motors

3.1 Introduction

In last chapter, a new analytical method for the design analysis of the SMPM motors has been proposed and discussed in detail. This chapter discusses the fabrication and operation of two types of the SMPM motors, .i.e., RF and AF for the validation of the proposed method. The development of the prototypes and the manufacturing difficulties has been briefly discussed. The operation of the developed machines with PM Enhanced sensing scheme with auxiliary motor and shadow coil has been reported. Section 3.2 describes the concept of rotor position sensing scheme in PM motors and various methods reported for the same. Section 3.3 and 3.4 deal with the development details of prototype RFPM and AFPM motors respectively. Section 3.5 depicts the initial results and waveforms obtained from AFPM machines developed. Section 3.6 summarizes the manufacturing difficulties involved in the manufacturing of prototype PM machines. The chapter is concluded in Section 3.6.

As discussed in Chapter 2, the proposed analytical method is applicable to both the RFSMPM and AFSMPM machines. The prototypes developed for the validation of the proposed method, are not a result of optimization process as it is subjected to the availability of the stampings and core for the stator, material for rotor and PMs. The development of the prototypes is rather inevitable because it is quite cumbersome to get exact design details of the commercially available PM motors worldwide. The next section discusses a novel sensorless rotor position sensing scheme for the prototypes and its merits over other approaches present for the same.

3.2 Rotor Position Sensing

The main advantage of the PM machines over conventional machines is the absence of the mechanical commutators and brushes. However, the electronic commutation of PMBL machines essentially require a rotor position sensor with which the commutation time and coil current can be controlled. In the initial stage of PM motor, with rotor position sensors the position of the rotor is sensed and the appropriate power electronics devices are switched ON/OFF for continuous rotation of rotor. The sensors generally used for rotor position sensing are Hall Effect sensors, Optical encoder and Resolver. These mechanical rotor position sensors have the drawback of increasing the number of connections between motor and controller, increased interference, limitation in accuracy of sensors due to environmental factors such as temperature, humidity etc., increased friction and inertia and require additional space in motor housing. With the application of PM motors in applications like space craft, aircraft engines, marine applications, such physical sensors are not suitable. For this reasons, sensorless techniques for the rotor position estimation of the PM motors have been encouraged.

The sensorless schemes are based on the indirect rotor position estimation. The reduction of cost and increase in reliability is the main reason to adapt sensorless schemes of rotor position estimation. A complete review of the sensorless techniques has been presented in [Pacas, 2011]. The properties of PM motors which vary with the rotor position are inductance, flux linkage and back-EMF [Ungurean *et al.,* 2010]. Inductance based methods are based on the change of reluctance in the air gap [Gabriel *et al.*, 2011a, 2011b]. Since this technique is based on the saliency of PM rotor, the accuracy of the rotor position detection depends only on the rotor geometry

[Bianchi *et al.,* 2007]. Back-EMF detection is the most common technique for rotor position sensing as reported in [Lai *et al.,* 2008; Lai *et al.,* 2011; Tsotoulidis *et al.,* 2011; Shao *et al.,* 2002]. Fig. 3.1 shows the different rotor position sensing schemes in literature.

The transient value of the back-EMF of each phase is related to the rotor position. For any back-EMF zero-crossing, rotor position can be known and no additional sensors are required [Shen *et al.,* 2003]. Free-wheeling diode [Ogasawara *et al.,* 1991] and third harmonic sensing [Jufer *et al.,* 1987] is used for the zero-crossing detection of the back-EMF, however, the hardware required is complicated. However, the simplest method to detect zero crossing of back-EMF is from terminal voltages or phase voltages in the stator winding [Serizawa *et al.,* 1987; Shen *et al.,* 1994]. The approach for sensing back-EMF with terminal voltages has been extended with PM Enhanced Sensing scheme of rotor position sensing [Srivastava *et al.,* 2013] for PMBL motors.

3.2.1 PM Enhanced Sensing Scheme

The scheme uses the concept of identical zero crossing of the back-EMF induced in the winding and the supply voltage. The motional induced EMF in the coil follows the path of flux density distribution in air gap. The back-EMF can be sensed either with two identical stators and rotors mounted on the same shaft or by providing the search coils in the stator having similar configuration of armature windings as that of primary windings.

A schematic of the PM enhanced sensing scheme has been shown in Fig. 3.2. When an auxiliary motor is used, the auxiliary stator stack length is less than that of main stator stack length [Srivastava *et al.,* 2013] while a shadow coil have few turns and configuration same as that of the main coils in the stator. However, due to the

drawbacks of back-EMF sensing using auxiliary motors as discussed in Section 3.3.5, the shadow coil technique has been encouraged than the auxiliary motor. The drawback of PM enhanced sensing scheme using auxiliary motor has been discussed in Section 3.3.5.

3.3 Radial Flux SMPM Motor

RFSMPM motors are the most common structures used for industrial purposes. The radial flux structures can be inner rotor or outer rotor. In present case, a 12-slot 12-pole outer hub rotor structure has been developed. In most brushless motors, windings are placed in slots in a laminated steel structure called the core. The purpose of the laminated steel is to channel more magnetic flux through the winding than would be possible with a non-ferrous core. While air core stators are preferred for high speed machines having flux weakening effect. A schematic of inner stator and outer hub rotor is shown in Fig. 3.3.

3.3.1 Inner Stator

The inner stator of a SMPM motor consists of stacked steel laminations. The stator stampings has semi-closed slots with the shaft and a key hole. Slot by slot stator windings are placed in these semi-closed slots. One or more coils are placed in the slots and they are interconnected to make a winding. Each of these windings is distributed over the stator periphery to form an even numbers of poles.

3.3.2 Outer Hub Rotor

The rotor is a simple outer hub rotor in which PMs are pasted on the inner surface of the rotor using a structural adhesive like Araldite or Loctite. Rare-earth parallel magnetized NdFeB PMs of alternate polarities are used. The outer rotor construction is considered superior to inner rotor construction because of ease of

installation and simple construction. This type construction is suitable for many applications like hybrid electric vehicle and PM wind generator [Chen *et al.*, 2005].

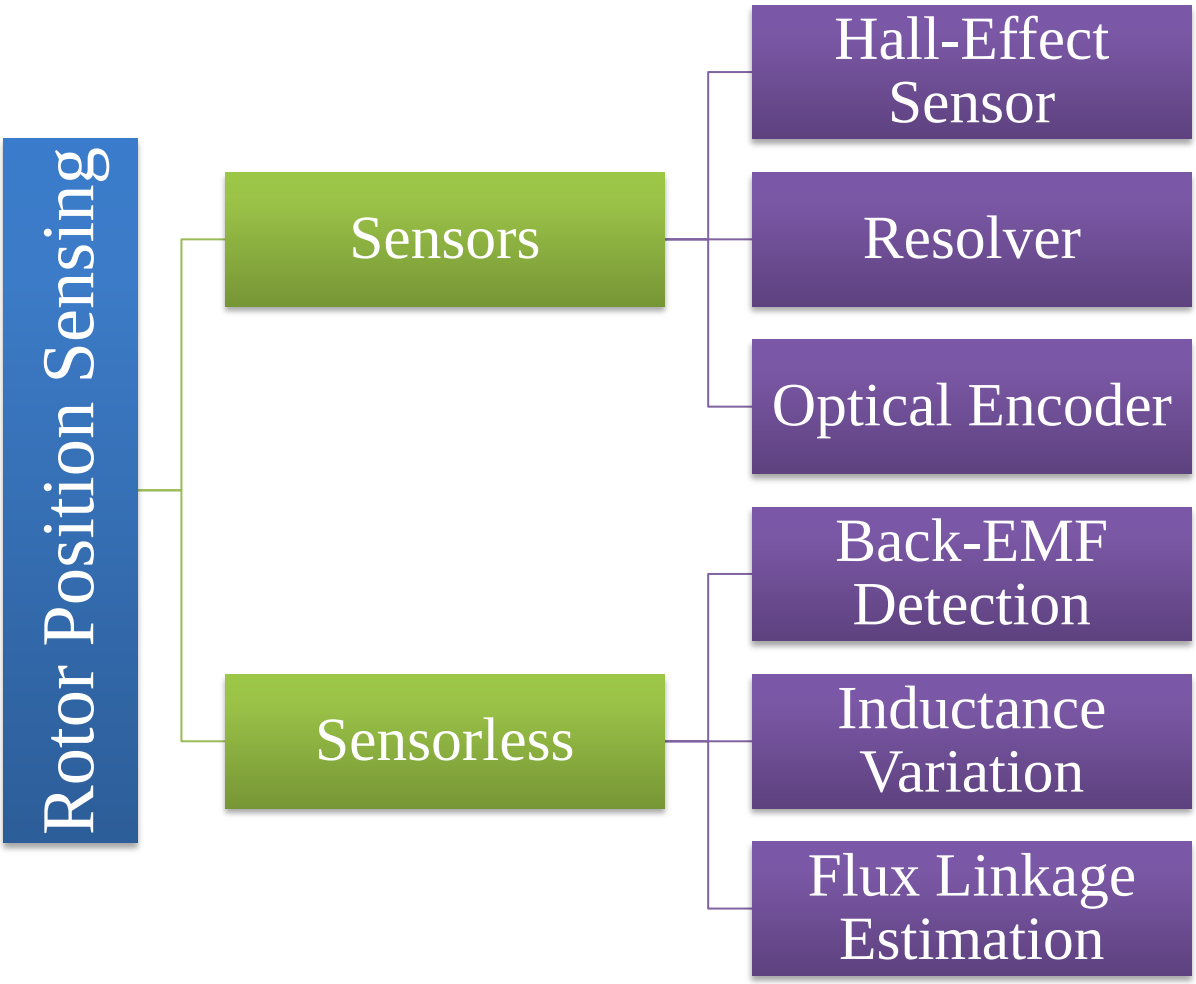

Fig. 3.1 Rotor Position Sensing Methods for PMBL Machines

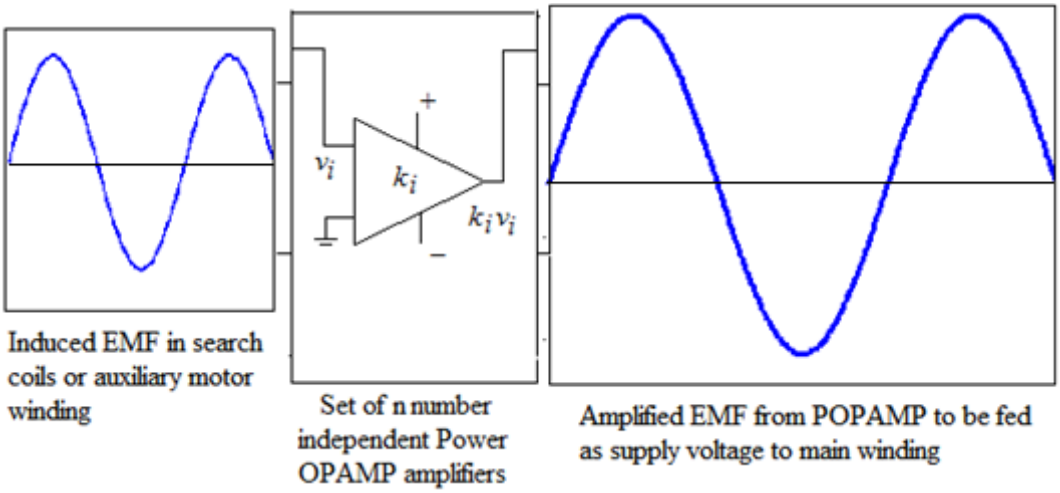

Fig. 3.2 PM Enhanced Sensing Scheme for Rotor Position Sensing

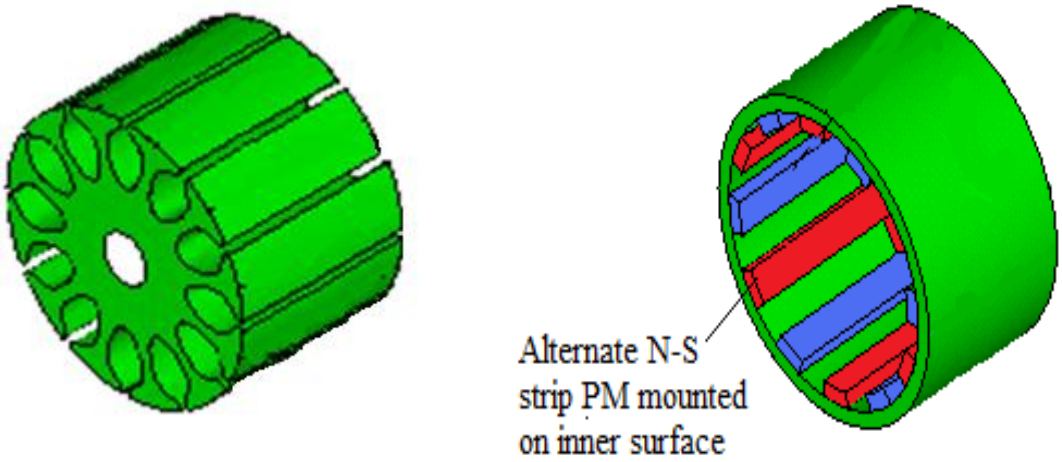

(a) (b)

Fig. 3.3 (a) Inner stator (windings not shown for clarity) (b) Outer Hub Rotor

3.3.3 Stator Winding

Several types of windings can be used in case of brushless PM machine like concentrated and distributed, single layer and double layer, etc. The conventional winding configuration of PM machines with concentrated windings has a number of slot per pole per phase of 0.5 and generally double layer configuration is used .i.e., one coil around each tooth leads to simple manufacturing. In present case, concentrated single-phase winding with one slot per pole has been used to match the rotor number of poles. The concentrated winding reduces the linkage flux and hence the inductance of the winding decreases. The overhang length decreases, thus the total ohmic loss also decreases. The fabricated prototype RFPM motor has been shown in Fig. 3.4.

3.3.4 Operation using PM Enhanced Sensing with Auxiliary Motor

The complete set up of the 12-slot 12-pole PM brushless machine is shown in Fig. 3.5. The POPAMP used for amplifying the auxiliary winding voltage is Texas Instruments LM675 operational amplifier having range of ±30V bias voltage supply and 3A maximum current rating. The details of POPAMPS used are given in Appendix-B. The details of the developed12-slot RFPM has been given in Table 3.1.

3.3.5 Drawbacks of PM Enhanced sensing using Auxiliary Motor

The PM enhanced sensing scheme has been initially used for rotor position estimation with the help of auxiliary motor provided on the same shaft as that of main motor. The present scheme provides proper commutation, however cannot provide starting torque. Secondly the scheme works perfectly for larger air gap, however for lesser air gaps, the armature reaction becomes dominant which is responsible for the change in zero crossing of the induced EMFs of main winding and auxiliary winding.

This resulted in braking torque for lesser air gap. Therefore, an alternative method of sensing the back-EMF using search coil has been attempted for AFSMPM machine.

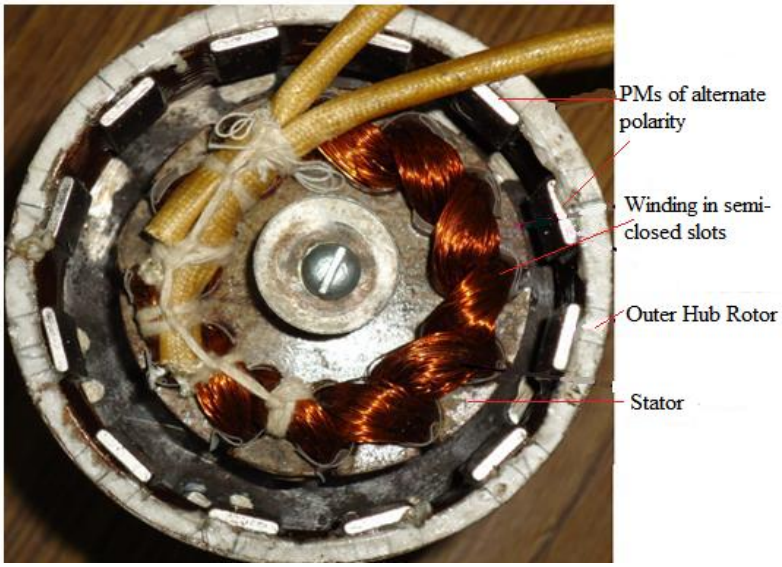

Fig. 3.4 Parts of the prototype RFPM Motor with larger air gap

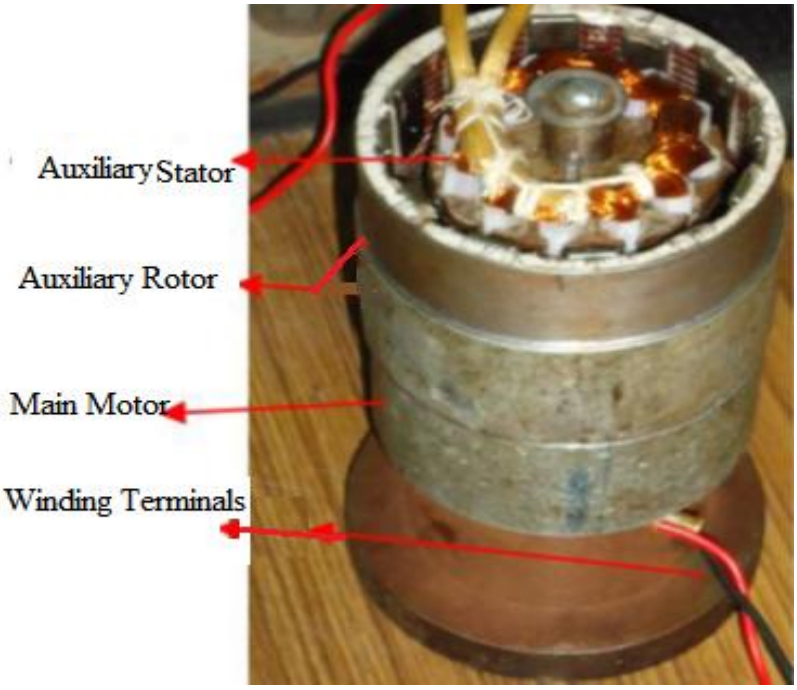

Fig. 3.5 Complete setup of the 12-slot 12-pole SMPM motor

3.4 Axial Flux SMPM Motor

AFSMPM machines have toroidal shaped cores, disc rotor and planar air gap. Flux crosses air gap in axial direction and passes round the cores in the circumferential direction. These machines can be designed as single-sided or double-sided; with or without armature slots; with or without armature core; with internal or external PM rotors; with surface mounted or interior PMs; and as single stage or multi-stage machines. The possible topologies available for the AFPM machines are:

- Single-sided AFPM machines [Yang *et al.,* 2013a, 2013b].
- Double-sided AFPM machines [Choi *et al.,* 2011*;* Sung *et al.,* 2012; Helmati *et al.,* 2015].
- Multi-stage AFPM machines [Caricchi *et al.,* 1996; McDonald *et al.,* 2011].

The single stator single rotor AFPM machines sets up a strong force of attraction which ultimately requires special arrangements [Aydin, 2010]. The double sided AFPM machine overcomes such drawback. Also the double stator single rotor machine employs less PMs and rotor material. The stator distributed winding leads to large overhang having a considerable copper length and as in these machines such the stator winding is not effectively utilized for production of torque. The single stator double rotor has an edge over all the configurations of the AFPM machines. Since both the working surfaces of the stator core is used, in comparison with both conventional machines and single rotor AFPMs, this structure allows the use of a higher percentage of the stator winding for the production of the machine torque. Furthermore, the two rotating discs act naturally as cooling fans. Therefore, the rotor structure is designed suitably removing heating in the machine stator due to copper and iron losses [Caricchi *et al.,* 1994].

For validation of the proposed analytical method discussed in Chapter 2, three prototypes of AFPM motor have been developed. Since, self-starting capability is the inherent drawback of the PM machines, a provision for providing the starting torque has been shown in Fig. 3.6. An arrangement with single stator and concentrated windings on both the active sides and PM rotor on one side and sheet rotor on the other side has been developed. An aluminum disc of 3mm is mounted on the rotor back iron to act as a sheet rotor induction motor. The sheet rotor Axial Flux Induction Motor (AFIM) starts operating by giving 3-phase supply. Once AFIM starts operating and bias supply is given to the POPAMP circuits, AFPM motor also starts functioning and 3-phase AC supply is also provided.

3.4.1 Single Sided Stator

The stator is sandwiched between the two rotors. It has circular slots on both the active surfaces. The stator is made up of electrical grade CRNO steel laminations and concentrated windings. The stator iron is laminated in the radial direction and resembles concentric toroidal ring. This makes the tooth flux density constant at any diameter on the stator due to a larger area available to carry the larger magnet flux. Though the torus construction for stators is simple and used in many applications but it uses more magnet weight because of the presence of additional air gap accommodating the windings. Axial-flux slotted machines have a lesser volume for a given power rating, making the power density higher as compared to the other configurations. The design details of the stator of three AFPM machines developed have been given in Table 3.1. In present case, two of the AFPM motor .i.e., Machine-B and Machine-C has semi-closed slots drilled as shown in Fig. 3.7 while Machine-D has open and trapezoidal slots.

3.4.2 AFPM Rotor

In AF machines, the annular active surface of rotor rotates in proximity to the stator with the flux crossing air gap in an axial direction. Rotor can be a solid thin disc or laminated core of mild steel supporting surface mounted PMs and shaft through it. In present case, a solid thin disc of 6mm has been used. The mechanical weakness and insufficient rigidness of laminated rotor makes it unsuitable for high-speed machines. A solid rotor though electromagnetically weaker than that of laminated rotor, still is physically superior [Mahmoudi *et al.*, 2013]. At high speeds, the solid rotors can be used with mechanical bearings, because it easily maintains its dynamic balance.

3.4.3 Axially Magnetized Permanent Magnets

Sector (arc) shaped NdFeB magnets are used for the developed axial flux PM machines whose dimensions are shown in Fig. 3.8. The remanent flux density of the PM materials is 1.0 T at 70°C. The designed NdFeB N35 PMs of required shape were imported from AIM Magnet Co., Ltd. The details of the arc PMs used have been given in Table 3.1. In AFPM machines, the actual magnet width is described as the magnet width to pole pitch ratio and can be defined as,

$$\alpha_p = \frac{w_{pm}}{\tau_p}$$

The magnet width varies along the machine radius. However, for AFPM machine with sector shaped PMs, accurate calculation results can be obtained if the average radius of the machine is considered as a computational parameter with trapezoidal slots [Shokri *et al*., 2015]. The magnets used for all the three configurations .i.e., Machine-B, C, D developed are same. The arc of the PM has an angular width of 60°. Though for 2-pole machines, 140°/160°is the proper angular width of the PMs. However, since these PMs were very costly, the studies with different arc pole have not been reported. A

schematic view of rotor disc without and with 4-pole and 6-pole PMs pasted on it can be depicted in Fig. 3.9. For safety critical applications where the operating temperatures are high, Loctite should be used for pasting the PMs, however the commercially available industrial adhesive Araldite has been used here which can withstand the temperature up to 80°C.

3.4.4 Winding Arrangement

Double layer concentrated slot-by-slot windings are used in developed prototype AFPM machines. The coils have rectangular shape according to the core cross section. The coils placed in the stator slots can be seen from Fig. 3.7. The axially-directed end-winding lengths are relatively short, yielding low resistance and reduced power loss. The active conductor lengths are the two radial portions facing the magnets, the polarities of which are arranged to induce additive EMFs around a stator coil. The slot star of winding arrangement for three axial flux configurations has been shown in Fig. 3.10. In addition to the main coils, shadow coils of few turns are also provided in the slots. The shadow coils are used to sense the back-EMF induced in each phase of the AFPM motor which are amplified using POPAMPs and fed to the respective main coils as supply to the machine. A complete set up of the experimental 6-pole AFPM 5-phase motor can be depicted from Fig. 3.11.

The speed induced EMF of each phase may be used for operation of the SMPM motors with H-bridge IGBT inverter as reported in [Lai *et al.,* 2011]. Since the IGBT/ MOSFET operates either at V=0 or at current I=0, the switching losses in H-Bridge are expected to be less. With rotor position sensing using Hall-Effect IC, the signal processing for each phase not only requires multiple components but also multiple bias supplies and additional supply for the opto-isolators. It was proposed to use commercially available low drift power amplifiers [Srivastava *et al.,* 2013]. The power

loss per IC is expected to be large; however its use simplifies the operation of the PM brushless motors in terms of number of components used. With only one POPAMP per phase, the overall loss decreases as compared to when power electronic circuits are used.

Table 3.1 Details of the Prototype SMPM Motors

SMPM Machine	**Machine-A**	**Machine-B**	**Machine-C**	**Machine-D**
Configuration	Radial Flux	Axial Flux	Axial Flux	Axial Flux
Number of slots	12	10	10	12
Number of Poles	12	4	6	4
Number of phases	1	5	5	3
Type of slots	Semi closed	Semi closed Circular	Semi closed Circular	Open Parallel Trapezoidal
Number of Turns per slot	120	120 (23 SWG)	140 (24 SWG)	120 (24 SWG)
Outer Diameter	0.075m	0.1523m	0.1523m	0.16m
Inner Diameter	0.057m	0.07615 m	0.07615 m	0.085m
Thickness of PM	4 mm	3 mm	3 mm	3 mm
PM Field Strength	0.1 T	1 T	1 T	1 T
Rated Current	0.5 Amp	2.5 Amp	2.5 Amp	3.0 Amp
Air gap	4 mm	12 mm	10 mm	10 mm
Resistance	40 Ω	3 Ω	3 Ω	12.55 Ω
Number of turns in search coil	20	10	10	8

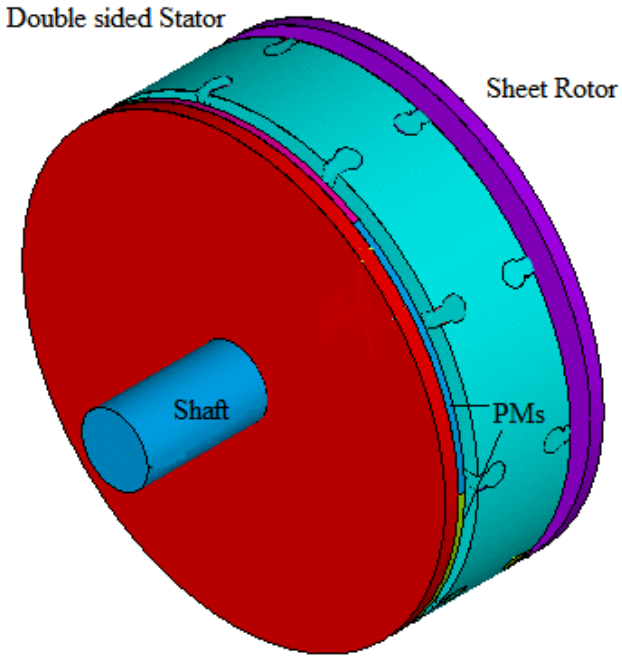

Fig. 3.6 Typical arrangement of the AFPM machine with PM rotor on one side and Al sheet rotor on the other

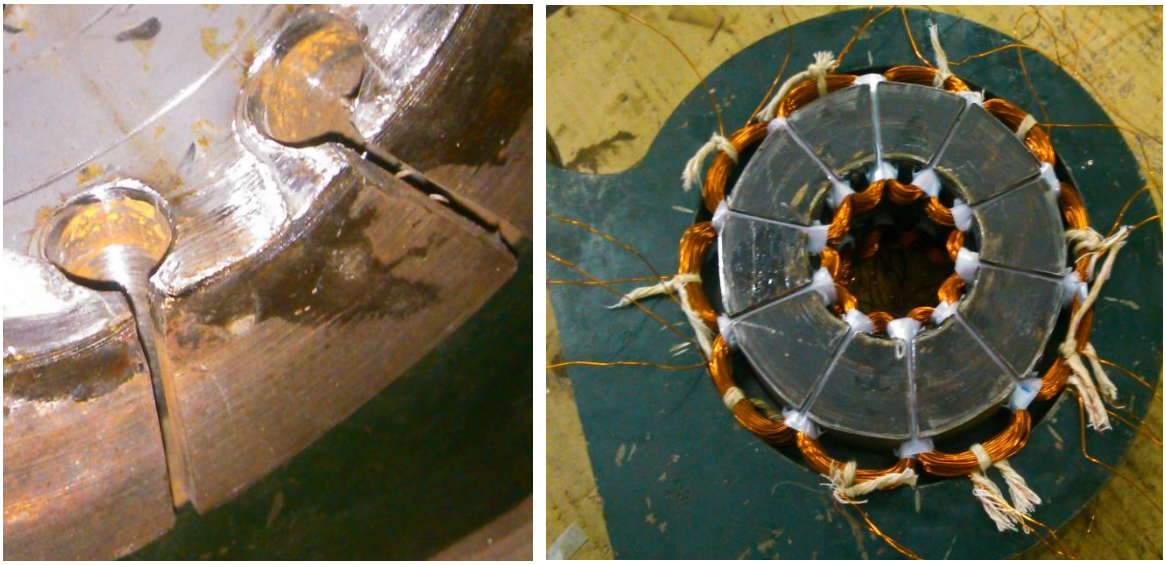

Fig. 3.7 (a) Stator with semi-closed slots (b) Stator with concentrated windings

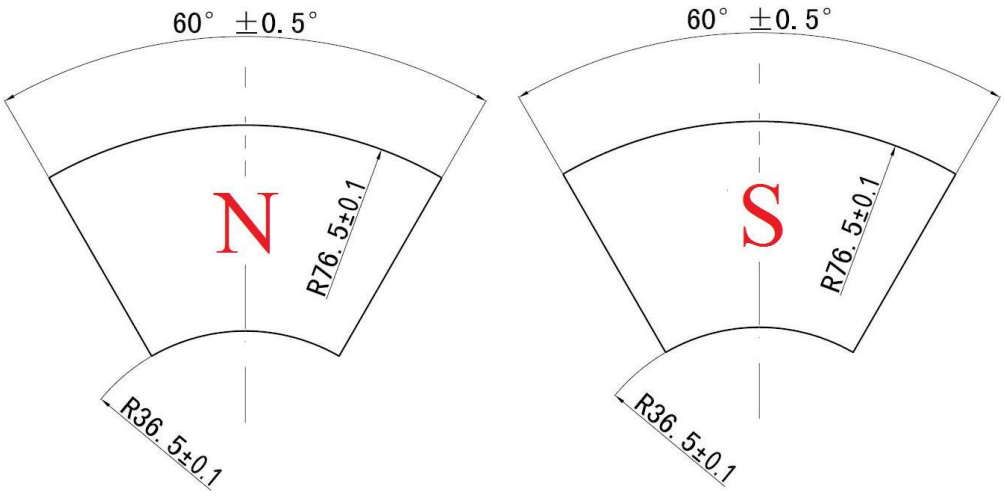

Fig. 3.8 Dimensions of arc shaped PMs used (all measurements are in mm)

(a)

(b)

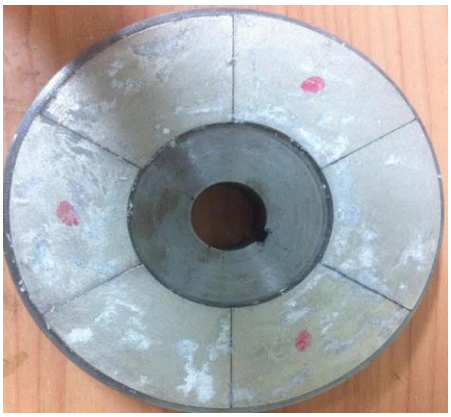

(c)

Fig. 3.9 (a) Soild disc Rotor (b) Four Pole PM Rotor (c) Six Pole PM Rotor

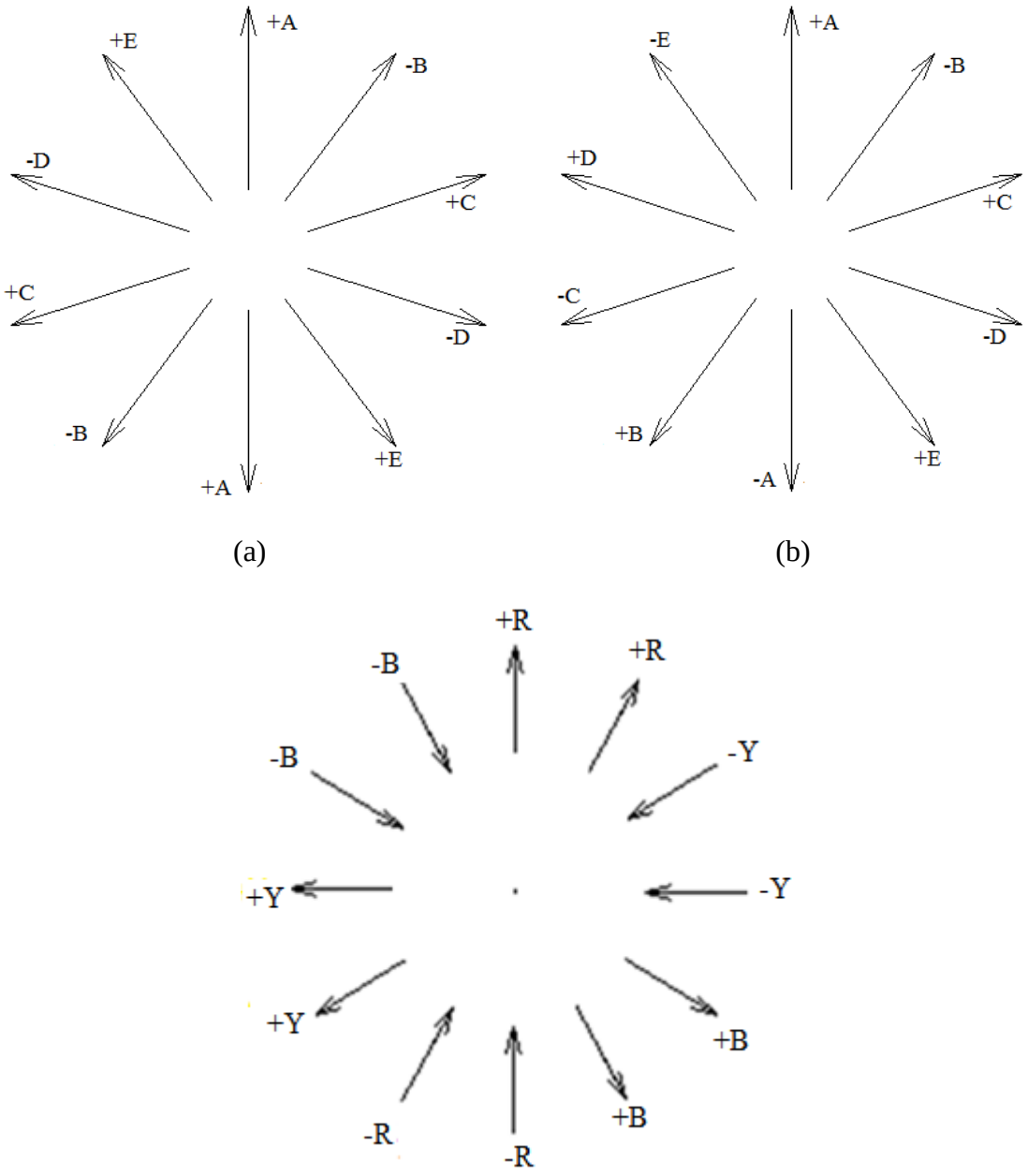

Fig. 3.10 Slot star of the windings (a) 5-phase 10-slot 4-pole (b) 5-phase 10-slot 6-pole (c) 3-phase 12-slot 4-pole

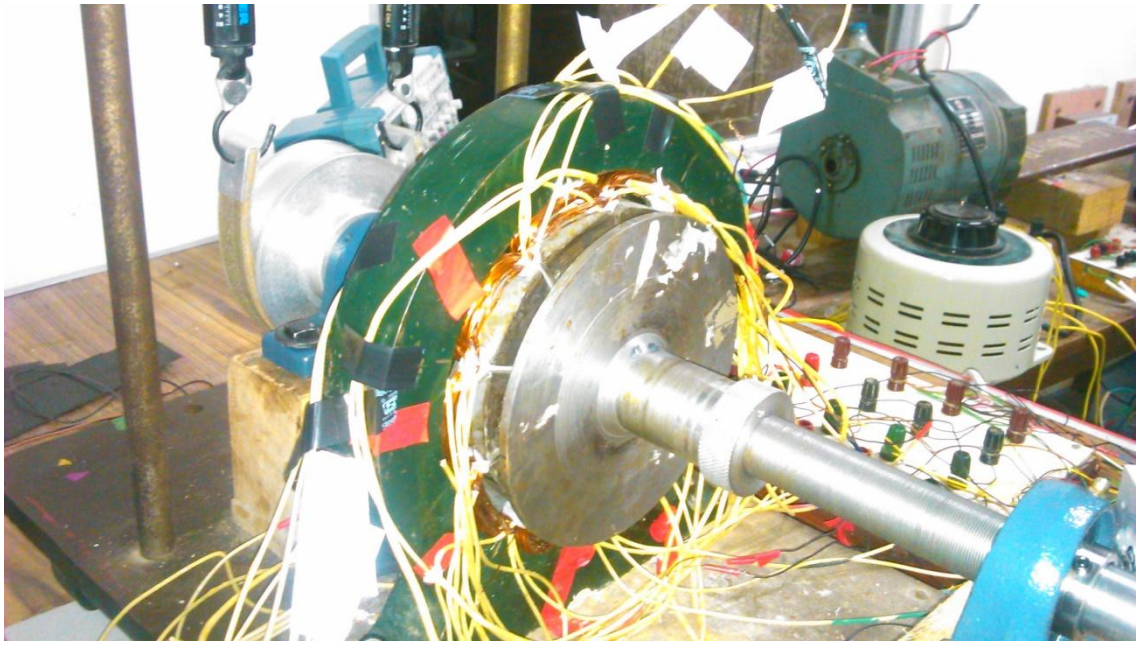

Fig. 3.11 Experimental set up of Machine-B

3.5 Preliminary Results

This section shows the preliminary results obtained from the prototypes developed. The speed induced EMF in auxiliary motor and main motor for RFPM and in search coil and main coil for AFPM machine has been shown when the machine is started as a generator. The effect of speed and air gap on back-EMF has been presented.

3.5.1 Machine-A

Initial results obtained from the RFPM motor are shown in Fig. 3.12 and Fig. 3.13. Fig. 3.12 shows the back-EMF induced in the main winding and amplified EMF of the auxiliary winding under no-load condition. It can be seen that the zero crossing of both the speed induced EMF and amplified EMF is identical and hence the amplified back-EMF from the POPAMPs can be supplied as input voltage to the main motor. Fig. 3.13 shows the amplified back-EMF and main motor winding back-EMF when the machine is loaded using frictional load.

3.5.2 Machine-B

The preliminary results obtained from the Machine-B have been shown. The EMF induced in the shadow coils and main coils are shown in Fig. 3.14 (a). The induced EMF is trapezoidal in shape due to concentrated windings in the stator. The zero crossing of the two EMFs is identical. The amplified EMF and the input current to main windings from POPAMP has been shown in Fig 3.14 (b). Fig. 3.15 depicts the induced back-EMF at two different speeds in the four phases out of five using four channel oscilloscope. It can be concluded from the Fig. 3.15 that as speed increases the EMF of the AFPM motor also increases. The effect of air gap on the induced EMF has also been shown in Fig. 3.16. With decrease in air gap the magnitude of the back-EMF increases at the same speed of 130 rpm. The peak-to-peak value of the amplified

voltage from the amplifier depends on the bias supply voltage. As the bias voltage increases, the peak value of amplified EMF also increases.

3.5.3 Machine-C

The induced EMF of the Machine-C and the current on load of the phases can be seen from Fig. 3.17. The speed induced back-EMF is a pure sinusoidal waveform. The effect of speed at common air gap and the effect of air gap at common speed on the induced back-EMF are depicted from Fig. 3.18 and Fig. 3.19 respectively. With decrease in the air gap, the flux density in the air gap increases and thus the speed induced back-EMF. However, with decreasing the slotting effect comes in picture and the machine back-EMF changes from sinusoidal to trapezoidal.

3.5.4 Machine-D

The 3-phase EMF induced in Machine-D when the machine is running as a generator using the AFIM motor present on the other side of the stator is shown in Fig. 3.20. The magnitude of the induced EMFs varies with change in the speed of motor. The main coil EMF and search coil EMF of the machine can be seen from Fig. 3.21. The waveforms are smooth and no ripples are present, this is due the presence of arc or sector shaped magnets in the disc rotor. While Fig. 3.22 shows the current waveform of Machine-D as a motor when loaded. The shape of current is not rectangular as it is influenced by the winding inductance and the induced back-EMF.

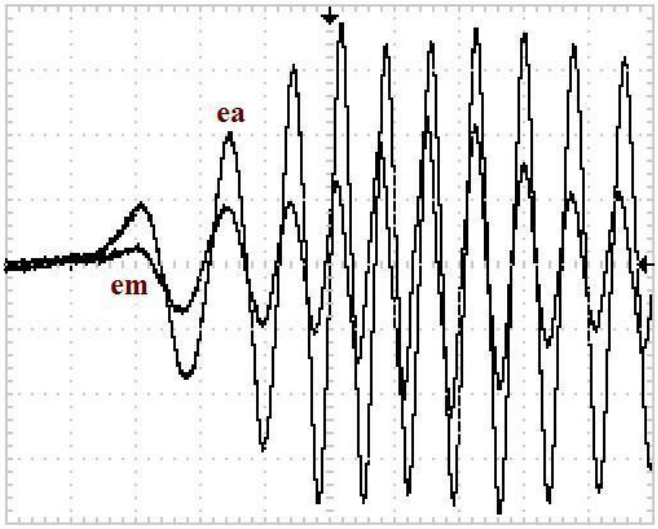

Fig.3.12 Amplified auxiliary winding EMF and main winding EMF (Time/div=100 ms, Volt/div=5 V) of Machine-A

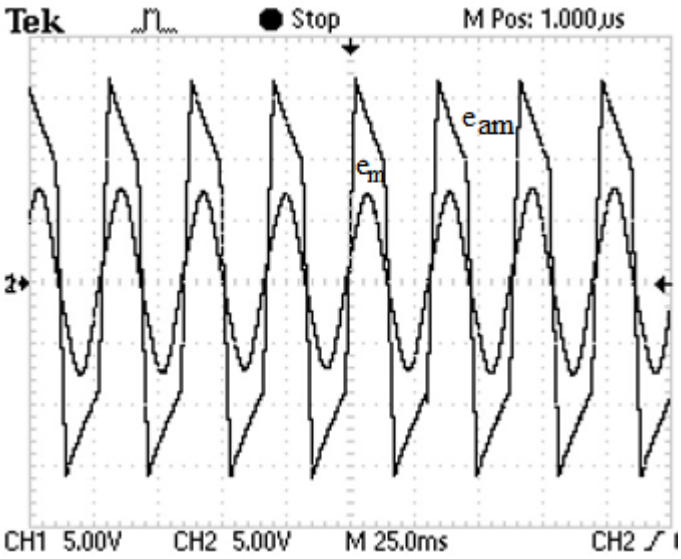

Fig. 3.13 Amplified auxiliary winding EMF and main winding EMF when machine is loaded (Time/div= 100 ms, Volt/div= 5 V) of Machine-A

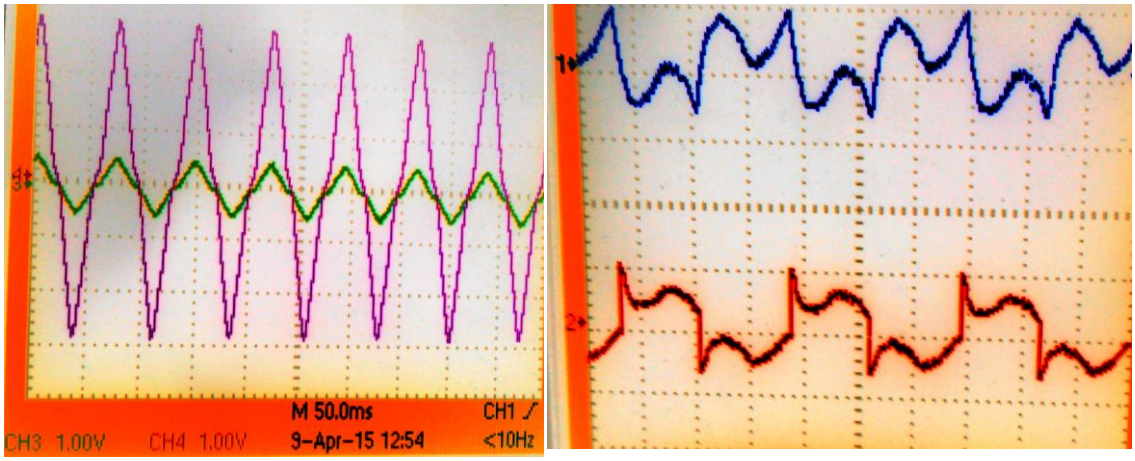

(a) (b)

Fig. 3.14 (a) Shadow coil and main winding EMF induced in the one of the phase of Machine-B (Time/div= 50 ms, Volt/div= 1 V) (b) Current and respective amplified EMF in one of the phase of Machine-B on load (Time/div= 5.0 ms, Volt/div= 15V, Amp/div=0.2A) *(5th phase not shown)*

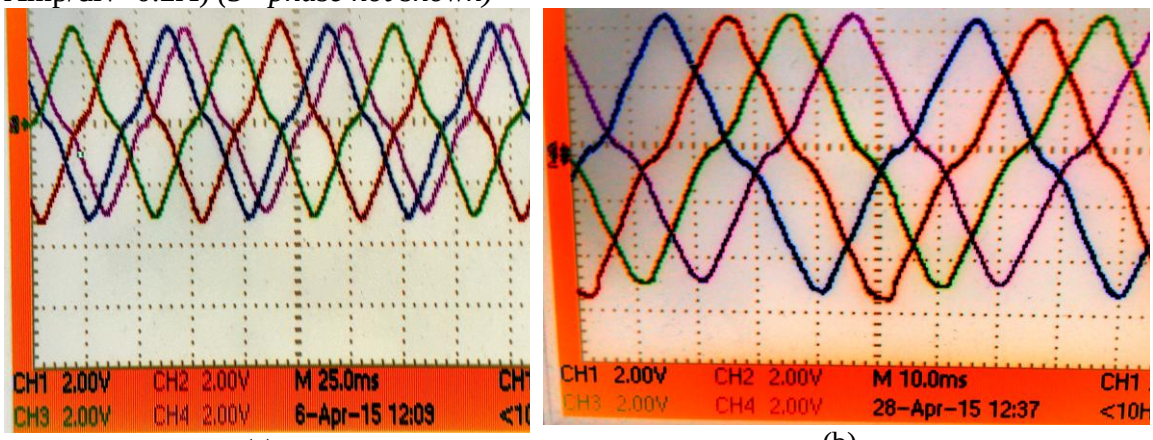

(a) (b)

Fig. 3.15 Speed induced EMF at (a) 130 rpm (Time/div= 25 ms, Volt/div= 2 V) (b) 618 rpm (Time/div= 10 ms, Volt/div= 2 V) *(5th phase not shown)*

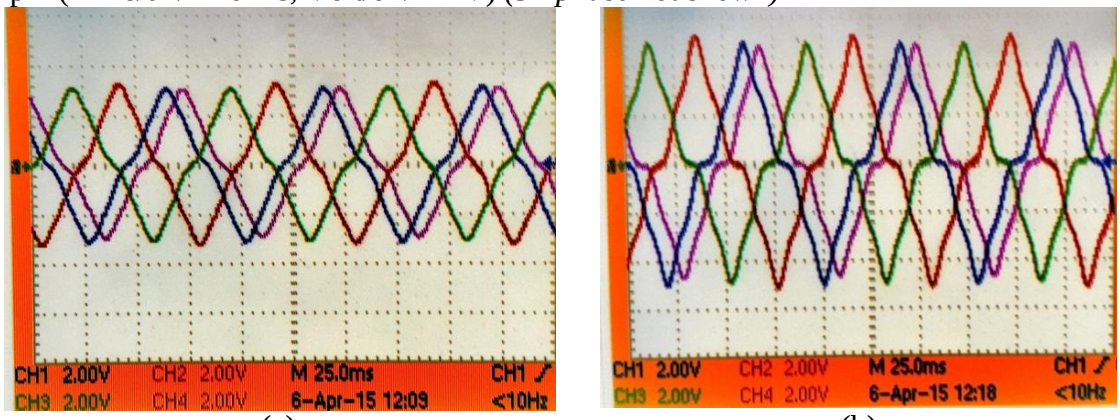

(a) (b)

Fig. 3.16 Effect of air gap on the induced EMF at (a) 12 mm (b) 9 mm (Time/div= 25 ms, Volt/div= 2 V) *(5th phase not shown)*

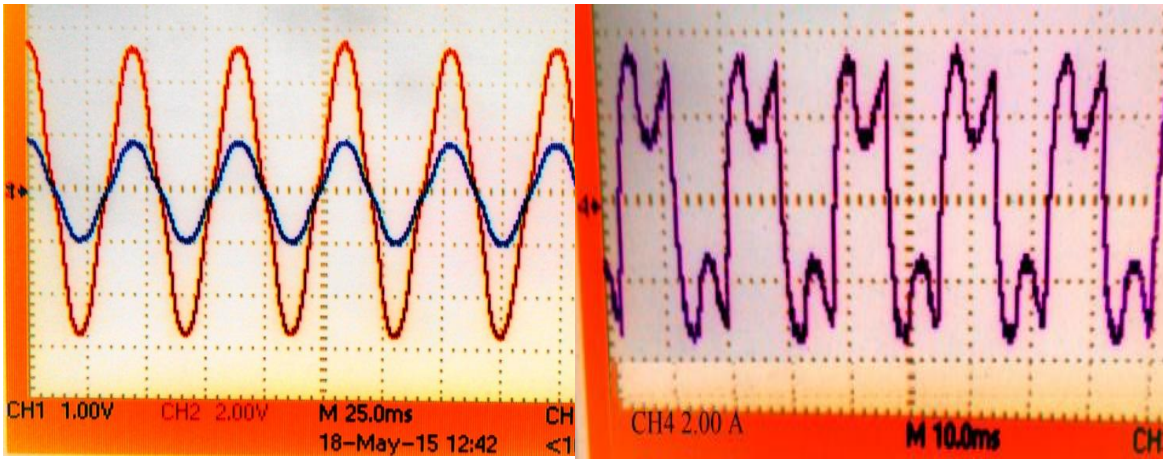

Fig. 3.17 (a) Shadow coil and main winding EMF induced in the one of the phase of Machine-C (Time/div= 25 ms, Volt/div= 1/2 V) (b) Current in one of the phase of Machine-C on load (Time/div= 10 ms, Amp/div= 0.2A) *(5th phase not shown)*

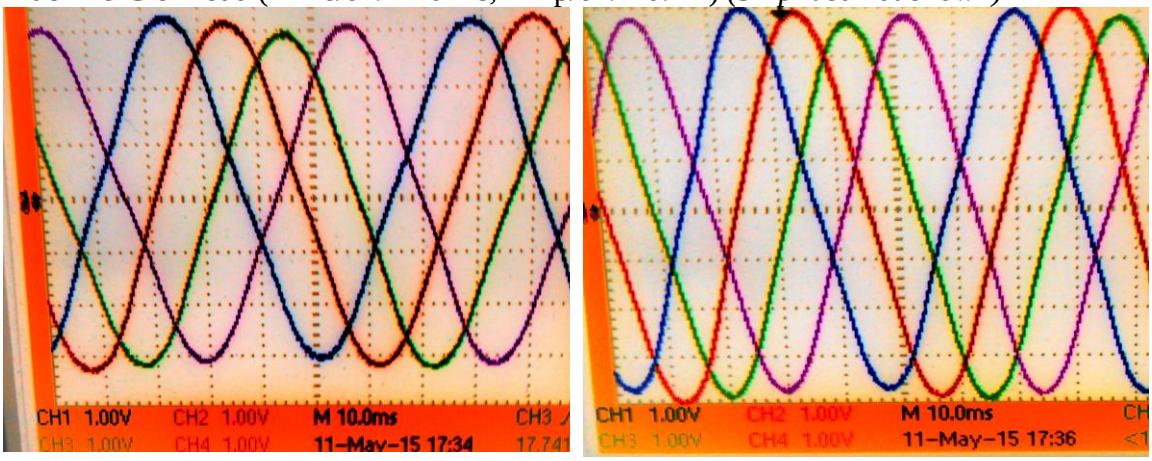

(a) (b)

Fig. 3.18 Speed induced EMF at (a) 370 rpm (b) 450 rpm (Time/div= 10 ms, Volt/div= 1V) *(5th phase not shown)*

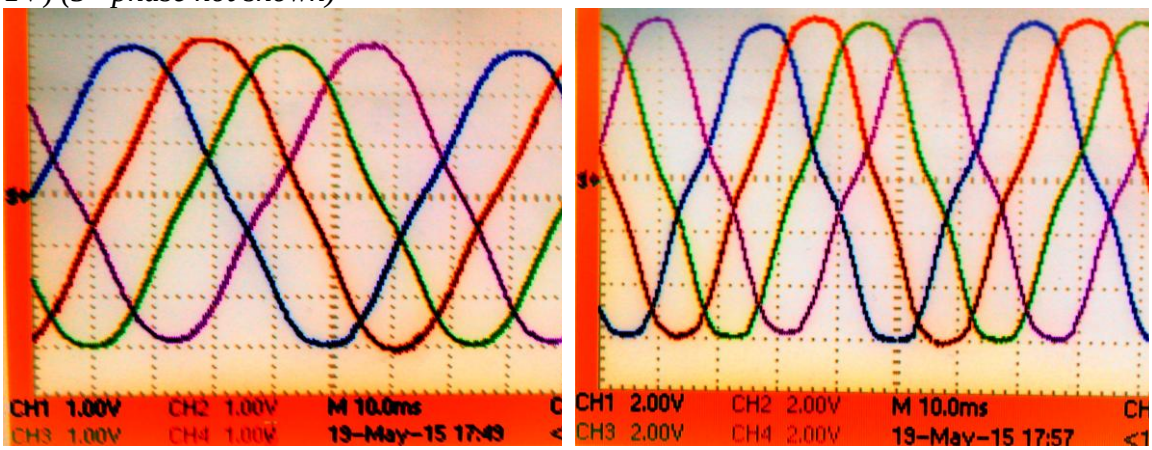

(a) (b)

Fig. 3.19 Effect of air gap on the induced EMF at (a) 15 mm (Time/div= 10 ms, Volt/div= 1V) (b) 11 mm (Time/div= 10 ms, Volt/div= 2V) *(5th phase not shown)*

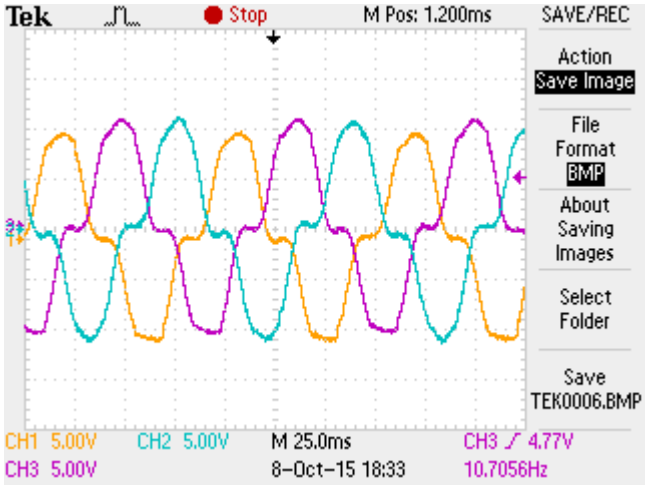

Fig. 3.20 Back-EMF induced in the main winding of Machine-D (Time/div= 25 ms, Volt/div= 5 V)

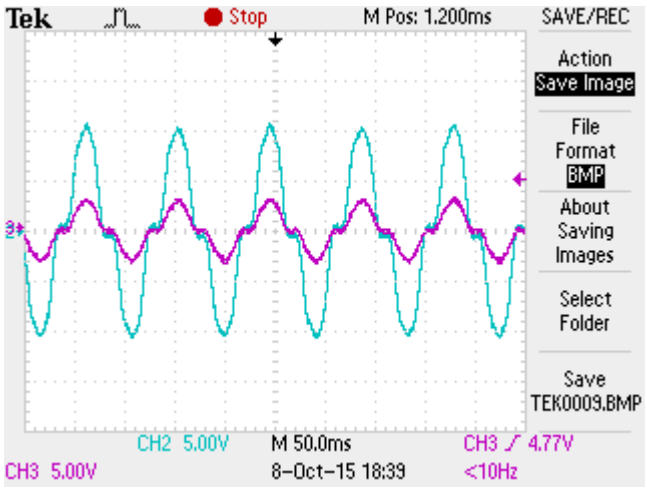

Fig. 3.21 Main coil EMF and search coil EMF of Machine-D (Time/div= 50 ms, Volt/div= 5V)

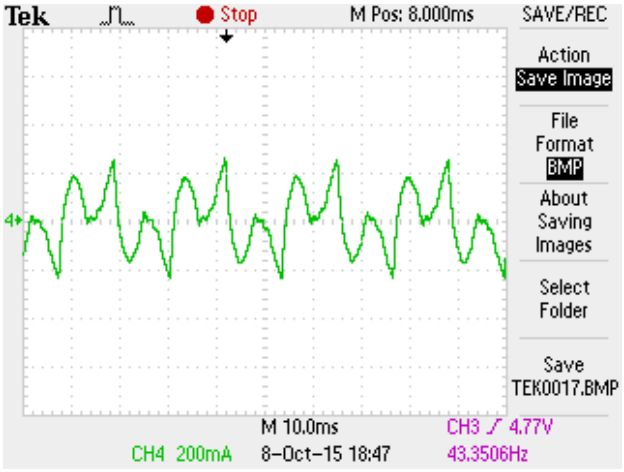

Fig. 3.22 Current waveform of Machine-D (Time/div= 10 ms, Amp/div= 0.2 A)

3.6 Mechanical Constraints in the manufacturing of the SMPM Machines

i. ***Pasting of PMs in RFPM and AFPM:*** The strong attractive force exists between the PMs of opposite polarity. The pasting of PMs of alternate polarity adjacent to each other on rotor disc is a challenging task. Only one PM can be pasted at a time which takes a lot of time especially when number of magnet poles are more in number.

ii. ***Asymmetric air gap:*** The PMs exert attraction force on the stator which leads to asymmetric air gap between rotor and stator.

iii. ***Unbalanced pull on rotor disc:*** For AFPM machines with single sided rotor as in the present cases, the main problem is the force exerted by PMs on the stator. The mechanical bearings should be strong enough to sustain the mechanical pull from the PMs. Centrifugal forces can cause mechanical stress on the rotating parts and the forces may break the structure. The centrifugal force F_{cen} acting on a magnet block glued at average radius r_{ave} may be calculated as [Parviainen, 2005],

$$F_{cen} = G_{PM}\omega^2 r_{ave}$$

The centrifugal forces depend on the mass of the permanent magnet, .i.e., the thickness of the permanent magnet affects the value of the centrifugal force.

iv. ***Drilling of the stator slots in axial flux stator:*** Since the stator core is made of laminated concentric sheets, the drilling of the stator slots in the core is a very tedious task. Appropriate arrangements should be made before drilling of slots in the stator core like placing a wooden log in the center of the core so that while the process, sheets should remain in their place.

v. ***Proper Fitting:*** For AFPM motor, fixing of PM rotor on one side is quite cumbersome. The PM rotor exerts very strong magnetic pull due to the presence of NdFeB magnets and tries to attract towards stator when current is supplied to the stator windings. Mechanical bearings which can bear this magnetic pull should be used along with proper fittings of the components.

3.7 Summary

Fabrication and operation of the SMPM machines for the validation of the proposed analytical method has been discussed in this Chapter. RF and AF configurations with surface mounted magnets has been fabricated in the workshop and assembled for the experimental set up. The concentrated windings have been used in all the configurations to avoid long overhang length, thus minimizing the copper losses. The concentrated windings have large p.u. inductance thus limiting short circuit current in the event of fault in the machine, thereby increasing the fault tolerance capability of the developed RFPM and AFPM machines. PM enhanced sensing scheme with shadow coils has been used for rotor position sensing and operation of the machines. The scheme is easy to implement as it uses one power operational amplifier per phase with no additional requirements of gate-drive circuit and is very less costly. The arrangement also adds fault tolerant capability to the machine. The preliminary results obtained from the developed machines have been shown. The next chapter deals with the results obtained from the experimental setups of different prototypes and their comparison with those obtained from the proposed approach for analysis of SMPM motors.